Rare earth-doped glass whispering gallery mode micro-lasers

Gabriele Frigenti, Simone Berneschi, Daniele Farnesi, Stefano Pelli, Giancarlo C. C. Righini, Silvia Soria, Yannick Dumeige, Patrice Feron, Davor Ristić, Francesco Prudenzano, et al.

Eur. Phys. J. Plus (2023) 138:679
https://doi.org/10.1140/epjp/s13360-023-04275-9

THE EUROPEAN PHYSICAL JOURNAL PLUS

Review

Rare earth-doped glass whispering gallery mode micro-lasers

Gabriele Frigenti[1], Simone Berneschi[1], Daniele Farnesi[1], Stefano Pelli[1], Giancarlo C. Righini[1], Silvia Soria[1], Yannick Dumeige[2], Patrice Féron[2], Davor Ristić[3], Francesco Prudenzano[4], Maurizio Ferrari[5], Gualtiero Nunzi Conti[1,a]

[1] Institute of Applied Physics "N. Carrara", Italian National Research Council, CNR-IFAC, 50019 Sesto Fiorentino, FI, Italy
[2] Institut FOTON (CNRS-UMR 6082), Université de Rennes 1, 22300 Lannion, France
[3] Division of Materials Physics, Laboratory for Molecular Physics, Ruđer Bošković Institute, Zagreb, Croatia
[4] Department of Electric and Information Engineering, Politecnico di Bari, 70125 Bari, Italy
[5] IFN-CNR CSMFO Lab. and FBK Photonics Unit, 38123 Povo, TN, Italy

Received: 1 March 2023 / Accepted: 12 July 2023

Abstract We review the works performed on whispering gallery mode (WGM) micro-optical resonators made in rare-earth (RE) doped glasses for implementing low threshold and narrow line coherent sources. These types of micro-lasers, because of their small size and ease of fabrication can be a useful tool for the characterization of laser glasses and have several applications, especially as sensors.

1 Introduction

Whispering gallery mode (WGM) micro-optical resonators are dielectric structures with cylindrical symmetry, like spheroids or toroids, having diameters below a millimeter, and in which light can be resonantly guided inside the dielectric material by total internal reflection [1, 2]. When properly activated, they represent an ideal resonant cavity to exploit lasing action as demonstrated in the pioneering work on Sm^{2+}:CaF_2 crystal spheres by Garret [3], which was followed many years later by those on micro-droplets of ethanol containing Rhodamine 6G [4], and in dye-doped polystyrene microspheres [5].

The first demonstration of high Q factor ($Q > 10^8$) glass WGM micro-resonators was done in fused quartz microspheres [6], and since then, WGM resonators made in highly transparent glasses have gained a great interest because they can be rather easily fabricated using melting and/or reflowing processes [7, 8], and they can be used for both the investigation of fundamental processes [9, 10] and for several applications in photonics [11–14]. Specifically, high-Q WGM resonators made in rare earth (RE) doped glasses represent an ideal and simple platform to implement narrow line, compact, and low threshold laser sources [15, 16]. Because of their small size and ease of fabrication, they can be a useful tool for the characterization of laser glasses [17] and represent an ideal platform for several sensing applications [18, 19]. Indeed, we focus our review on WGM micro-lasers made in RE doped glasses, we describe their fabrication processes and their characterization including lasing threshold, RE dopant, emission wavelength. Since the first demonstration, which was done in neodymium-doped silica microspheres [20, 21], the vast literature that followed includes resonators with different shapes (microspheres [20], microdisks [22], microtoroids [23], microbottles [24], etc.), RE dopants (Er^{3+} [25], Er^{3+}:Yb^{3+} [26], Nd^{3+} [20], Tm^{3+} [27], etc.), and glass matrices (silica [21], tellurite [28], phosphate [26], fluoride [29], etc.). This work ends presenting the unique advantages of active glass WGM resonators for applications in sensing.

2 Fabrication

The techniques to fabricate WGM micro-resonators in RE doped glass are similar to those used for undoped glass and are based on melting and/or reflowing submillimeter glass powders or tips. Depending on the glass type (silicate, phosphate, germanate, tellurite, chalcogenide, etc.), the right temperature has to be selected above the glass transition temperature but still keeping high viscosity so that surface tension can provide a spheroidal shape [7]. Additionally, the resulting 'fire polished' surface typically has very low roughness (RMS < 50 nm [6]), thus avoiding complex mechanical polishing, which are required for crystals [30], or semiconductors [31]. In fact, the total intrinsic Q of a WGM resonator is determined by contributions from curvature losses ($Q^{-1}{}_{\mathrm{rad}}$), material losses ($Q^{-1}{}_{\mathrm{mat}}$) and surface scattering losses ($Q^{-1}{}_{\mathrm{scat}}$) according to the equation: $Q^{-1} = Q^{-1}{}_{\mathrm{rad}} + Q^{-1}{}_{\mathrm{scat}} + Q^{-1}{}_{\mathrm{mat}}$ [1]. $Q^{-1}{}_{\mathrm{rad}}$ vanishes exponentially with resonator size (for instance, for a sphere of diameter d, if $d/\lambda \geq 15$ than $Q_{\mathrm{rad}} > 10^{11}$) while $Q^{-1}{}_{\mathrm{mat}}$ is inversely proportional to the absorption coefficient α, and $Q^{-1}{}_{\mathrm{scat}}$ is inversely proportional to the square of roughness RMS

[a] e-mail: g.nunziconti@ifac.cnr.it (corresponding author)

Published online: 03 August 2023

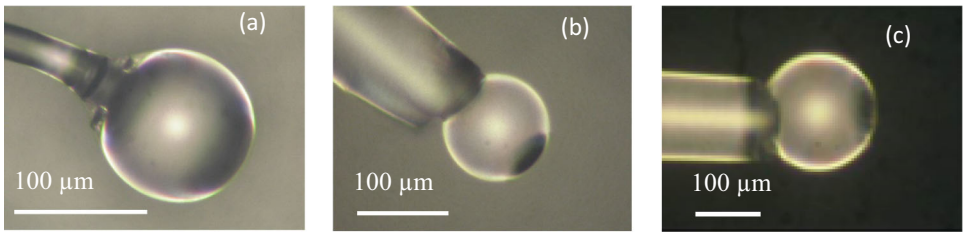

Fig. 1 Images of microspheres fabricated in Er^{3+}-doped glass. **a** Phosphate glass sphere fabricated by melting the tip of a glass wire to which it is kept attached; **b** phosphate glass sphere fabricated by melting glass powder; **c** silica sphere produced by the sol–gel route. Spheres **b** and **c** are both glued to the tip of a fiber for handling

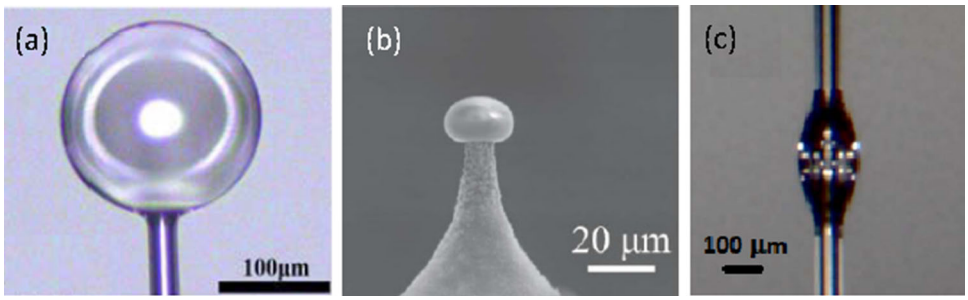

Fig. 2 Images of Er^{3+}/Yb^{3+} codoped glass micro-resonators. **a** Tellurite glass microbubble (from [42]); **b** SEM image of a silica spheroid fabricated on a silicon chip (from [65]); **c** phosphate glass microbottle made on a silica glass wire (from [24])

[1]. Therefore, WGM resonators with extremely high optical Q factors ($Q \geq 10^8$) can be easily obtained in low loss glasses, and outside the absorption band of the RE (where the so-called 'cold' Q factor is measured). It is worth pointing out that, for the lasing performances, the chosen type of glass matrix (silica, tellurite, phosphate, fluoride, etc.), strongly affect the RE solubility and phonon energy [21, 26, 28, 29].

2.1 Bulk glass resonators

In the seminal paper by Braginsky et al. [6], silica spheres with diameters in the range 40–400 µm were fabricated on the top of short fused quartz stems of different diameters. Upon heating the glass tip above the transition temperature, the glass reflows forming a spherical shape under the influence of surface tension and, if the glass viscosity is kept high, the reflowed structure is highly spherical with eccentricities e of the order of 1–2% [1]. Several heat sources can be used for heating the glass including gas torches [32], high power lasers (like CO_2 for silica) [33], electric arcs [34], and resistive microheaters [35]. Indeed, this simple method can be applied to any type of RE glass rod or wire or to a fiber and allows a good control of the microsphere diameter. If only the fiber core is doped, the cladding has to be removed prior to heating, at least partially, and this process typically requires a combination of mechanical machining and chemical etching [36, 37]. The sphere is left attached to the glass stem (see Fig. 1a), which can be used for easy handling. A drawback of this method is that only one resonator at a time can be fabricated.

Similarly, high Q WGM microbubble and microbottle resonators can be fabricated from RE-doped silica glass fibers or wires. Microbubble lasers [38] were made on active fibers using the so-called "soften and compress" method [39, 40]. This shape allows unique potentials for implementing low threshold, and high efficiency micro-lasers, as modeled in Ref. [41]. Microbubble lasers fabricated from RE doped capillaries made in tellurite glass have been demonstrated (see Fig. 2a) [42].

Glass microspheres or microtoroids can be fabricated on a chip, typically using silica on silicon wafers. Sol–gel technology is mainly used to deposit RE-doped silica glass thin films on the wafer. Indeed, sol–gel chemistry is a well-known, flexible, and convenient method for producing optical materials with enhanced performances, and moreover it allows precise control of the RE dopant concentration [43]. Films are deposited by spin coating and then disks are patterned by standard lithography and buffered oxide wet etching. The underlying silicon is then chemically etched using XeF_2, leaving RE doped silica disks supported by silicon pillars. Finally, a CO_2 laser is used to reflow the silica micro-disk to form a smooth microtoroid [44] or microsphere [45], with diameters of few tens of microns (see Fig. 2b for an on chip microsphere). Alternatively, direct femtosecond laser micromachining of RE doped glass substrates allows the formation of 3D structures like microdisks supported by thin pillar, which are then shaped into spheroids by using again a CO_2 laser reflow step [46]. In this review, we consider on chip 3D micro-optical resonators whose level of integration does not include coupling to an planar waveguide [47, 48].

A different approach to fabricate many microspheres at the same time is based on crushing a piece of (RE doped) glass in powder of submillimeter grains and then dropping them through a microwave plasma torch [49]. The glass grains are melted and they acquire spherical shape by surface tension before being collected a few tens of centimeters below the torch. By adjusting the microwave

power and the noble gas flow, it is possible to reach the desired temperature within a wide range up to 2000 °C and to produce spheres of different sizes (from 10 to 200 μm in diameter depending on the powder size), with a very low eccentricity e ($e < 10^{-4}$). A similar approach uses an electric tube furnace, which operates at a lower temperature of up to 900 °C [50]. A third approach to fabricate free spheres consists of melting the oxide components in a furnace and dropping the viscous glass on a spinning plate [51]. The melted glass is spun out by centrifugal force and cooled down quickly, forming microspheres with a diameter ranging from several micrometers to several hundred micrometers. A disadvantage of these techniques is the large size distribution of the microspheres, which are difficult to manipulate and need to be picked up properly one by one, typically gluing them on the tapered tip of a fiber (see Fig. 1b, c).

A specific protocol has been developed by the authors to directly fabricate sol–gel silica spheres incorporating rare earths into the glass. By using acid catalysts, silica microspheres are fabricated with different diameters, ranging from a hundred nanometer to approximately 150 μm, always with a very high surface quality (see Fig. 1c) [52].

2.2 Glass coating-based resonators

A different approach to implement WGM micro-lasers is that of depositing an active layer on a high-Q passive resonator, i.e., a microsphere [53], a microtoroid [54], a microbubble [55] or a microbottle [56], typically made in silica. In this configuration, the RE ions are only inside the layer, whose thickness can vary from few hundreds of nanometer up to few microns. Sol–gel technology allows making very high quality glass films by the dip-coating method using several steps in order to obtain the desired thickness of the film [57]. Another method consists of depositing a thin layer of melted RE doped glass-like Er^{3+}/Yb^{3+} codoped phosphate glass-on a silica microsphere [58]. The much lower melting temperature of the phosphate glass compared to silica easily allows using this procedure. Similarly, microbottle shaped lasers can be made by using a CO_2 laser to melt Er^{3+}/Yb^{3+} codoped phosphate glass directly onto silica microcapillaries or wires, as shown in Fig. 2c [24]. Finally, a special case is that of a thin layer of RE doped glass formed by high-energy ion implantation. Er ions have been implanted on high-Q silica on silicon microtoroids [23, 59] and microdisks [22], and on silica microspheres [60], using different energies and fluencies. Very recently, integrated white-light lasers have been demonstrated in high-Q silica microtoroids coated with silica sol–gel containing $CaF_2{:}Yb_{35}Tm_{1.5}Er_{0.5}$ nanocrystals [61]. Multiple lasing bands have been also obtained with PMMA assisted Er^{3+}/Yb^{3+} co-doped ultra-high Q silica microspheres [62]. Similarly, liquid-based surface doping technology [63] has been recently implemented on silica microspheres to uniformly introduce Er^{3+} ions while keeping ultra-high quality factor [64].

3 Characterization

3.1 Coupling

In order to characterize active RE-doped WGM resonators, the best approach to efficiently couple pump light as well as to collect the output signal is based on phase-matched evanescent coupling and requires some overlap of the field of the WGM with the field of the coupler. The main coupling tools are waveguides such as tapered optical fibers [66] or integrated waveguides [67], or prisms [6] if free space optics is used. Two different fiber couplers for pump and signal can be used to optimize the coupling at both wavelengths [68], as sketched in Fig. 3 for an Er^{3+} doped microsphere. A half taper is used to couple the pump, while a second taper collects the signal (both the co-propagating and counter propagating one), with an output coupling efficiency that can be varied by changing the taper-resonator distance (as an output mirror with variable transmission). Figure 3 also shows the pump source operating either at 980 nm or at 1480 nm for the case of Er^{3+} ions. By using a finely tunable narrow line source, resonant pumping can be implement to improve the efficiency of the process and further lower the lasing threshold [23, 59]. The fiber-coupled signal spectrum around 1550 nm is collected using an optical spectrum analyzer (OSA). Different coupling regimes can be observed in active resonators by increasing the pump coupling rate from undercoupling to selective amplification, before lasing action takes place, as it has been done for Nd^{3+} [69] and Er^{3+} doped [70] glass microspheres.

In a different approach, a special hybrid taper can be designed to optimize both pump and signal coupling [71]. Finally, a single half taper can be used to couple the pump and at the same time collect the counter propagating signal [72], and this approach has been exploited to implement miniaturized optical microwave sources using a dual-wavelength microlaser [73]. A similar architecture can be implemented using an optical nanoantenna made on the tip of a fiber, which is able to couple the pump and at the same collect the counter propagating signal from the resonator [74].

Prism-based coupling (see Fig. 4a) is quite robust and conveniently allows phase matching, but for efficient coupling it also requires mode matching of the far field free space pump beam with the WGM [75], which can be rather critical. Free-space coupling of a tangential beam into WGMs (see Fig. 4b) by using a microscope system is a robust and convenient approach, but it is extremely inefficient because of the large phase and mode mismatches, which can be quantitatively predicted [76]. The coupling efficiency to a high refractive index microsphere can be improved by using a ‘terrace’ structure made with a lower refractive index sol–gel [77, 78], as sketched in Fig. 4b. The beam is focused on different positions of the terrace to maximize the fluorescence/lasing emission

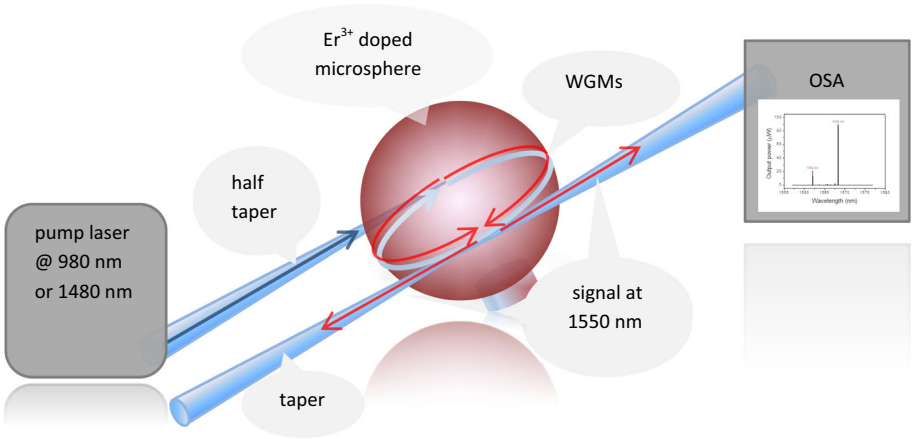

Fig. 3 Setup for Er^{3+} doped glass WGM micro-resonator characterization. A half taper is used for pumping the WGM microsphere by using a fiber pigtailed laser operating either at 980 nm or at 1480 nm. A second fiber taper collects both co-propagating and counter propagating signals around 1550 nm [68], which are then sent to an optical spectrum analyzer (OSA)

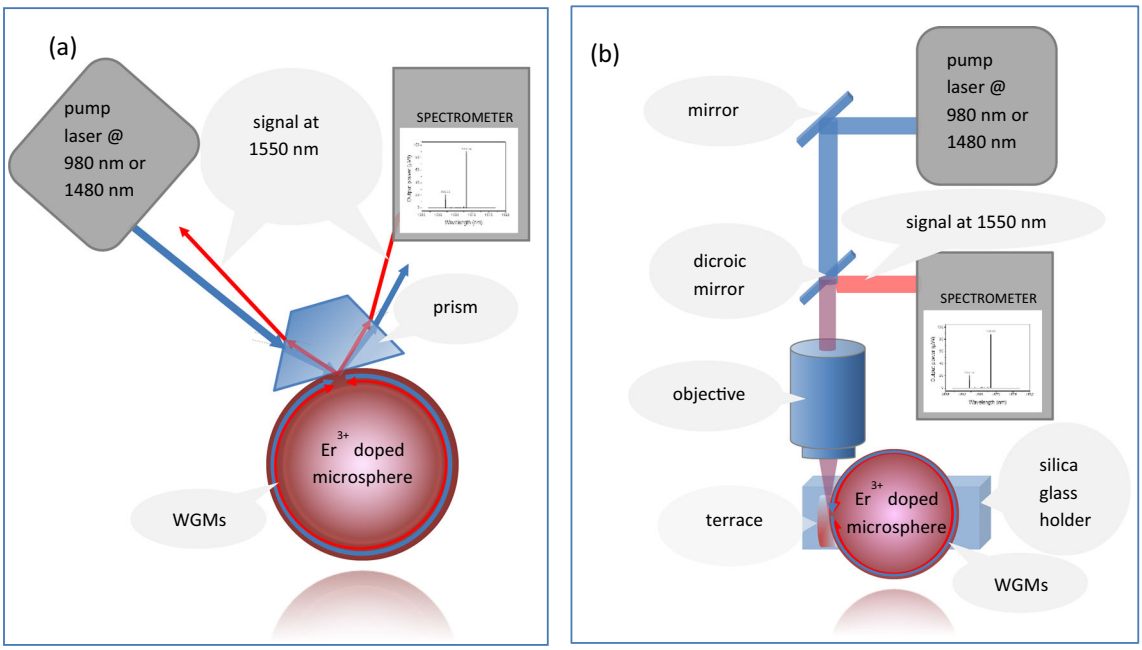

Fig. 4 Setup for active (Er^{3+} doped) WGM resonator characterization based on **a** prism evanescent coupling and **b** free space coupling using a microscope. Collimated or focused beams from the pump lasers are used, while output signal beams from the microspheres are sent and analyzed with a spectrometer. In **b** the counter propagating emission spectrum is collected with the same objective used for the excitation. A 'terrace' structure made of a sol–gel with lower refractive index compared to the glass can be attached to the sphere and used to improve pump coupling and to enhance the emission as compared to the uncoated sphere [77]

from the counter propagating microsphere WGMs. In both the approaches of Fig. 4a, b, free space signal beams are collected and analyzed with a spectrometer.

3.2 Spectroscopy and lasing

Cold-cavity Q factors, which are measured outside the absorption band of the RE ions, are typically in the range between 10^5 and 10^7 [32], but values up to 10^8 have been also measured [62, 79, 80]. An example of a 'cold' resonance measured in a microsphere of 75 μm in diameter made in a sodium–alumino–phosphate glass doped with 1.5 wt% of Er_2O_3 and 3 wt% of Yb_2O_3 is shown in Fig. 5a. The fine wavelength scan is performed around 1.6 μm, which is at the edge of the absorption band of the $^4I_{13/2}$ level ($\sigma_{abs} = 0.35 \times 10^{-21}$ cm^2). The corresponding resonance Q value of 0.8×10^6 is in agreement with that calculated taking into account only the residual material absorption at that wavelength [32].

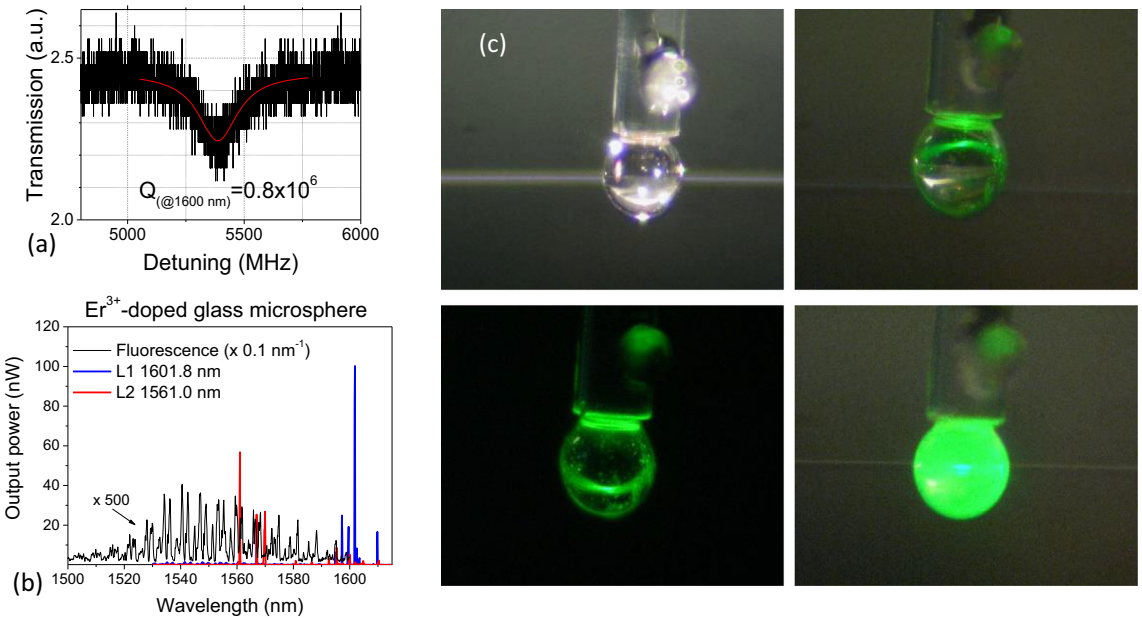

Fig. 5 **a** WGM resonance measured around 1600 nm of a 75 μm microsphere made in an Er^{3+}/Yb^{3+} codoped phosphate glass and **b** WGM emission spectra including fluorescence spectrum below lasing threshold (black line), and lasing spectra corresponding to the maximum (blue line) and the minimum (red line) wavelength peak values; **c** image of an Er^{3+} doped phosphate microsphere with a diameter of 150 μm, and **d**–**f** of the green upconversion appearing after pumping at 980 nm, and mapping several different WGMs, depending on the excitation taper position (barely visible in the back, see also text)

RE doped spectroscopic properties are typically assessed on the bulk glass before the second melting occurs to shape the WGM micro-resonator. We have performed characterization of the spectroscopic properties of Er^{3+} ions after microsphere fabrication and compared these properties with those of bulk glass We found that photoluminescence spectra of the $^4I_{13/2} \rightarrow {}^4I_{15/2}$ transition of Er^{3+} ions after pumping at 980 nm, as well as the corresponding experimental lifetimes measured in the precursor glasses and in the corresponding microspheres can be dissimilar. Up to a doubling of the effective bandwidth and almost a halving of the lifetime was measured on the microsphere as compared to the bulk glass. Site-to-site inhomogeneities, most probably due to the fabrication process, can modify the local environment of the Er^{3+} ions in the microsphere, resulting in significant modification of the transition probability among the Starks levels. The experimental setup used for measuring the radiative lifetime of Er^{3+} ions in microspheres is the same typically used for the precursor bulk glass [81].

Typical emission spectra around 1550 nm of an Er^{3+} doped phosphate glass microsphere (with a diameter of 75 μm) are shown in Fig. 5b. We used a setup similar to the one sketched in Fig. 3, with the signal output coupled to a tapered fiber, which is then connected to an OSA. By switching the 980 nm or 1480 nm pump laser on, we first observed the typical Er^{3+}-ions fluorescence spectrum with a series of peaks that can be assigned to several families of WGMs [82]. When increasing the pump intensity above a certain threshold we obtained laser oscillation, which results in a sudden increase in the output in narrow peaks at just one or few wavelengths. By varying the contact position of the tip of the half taper fiber coupler relative to the sphere and increasing the pump power the lasing spectrum moved toward WGMs of shorter wavelength. In fact, when the pump power is increased, the blue shift, which is due to the shift toward shorter wavelengths that occurs in the Er^{3+} gain spectrum peak when the inversion rate increases [83], effectively dominates on the thermal induced red shift. Figure 5b shows the two lasing spectra corresponding to the maximum (1601.8 nm) and the minimum (1561.0 nm) wavelength peak values we were able to obtain in this microsphere. The covered range is about 40 nm broad.

Figure 5c shows a collection of images on how an Er^{3+}doped glass microsphere typically appears under an optical microscope, when pumping it at 980 nm. In the first picture, behind the microsphere, which is about 150 μm in diameter, we can spot the coupling taper, slightly out of focus and not yet in contact with the resonator. In the other three pictures, depending on the taper position different WGMs are excited, whose spatial distribution can be mapped thanks to the green upconversion [1, 84]. Interestingly, in the last image several modes are simultaneously excited, including those with higher azimuthal mode number, resulting in the appearance of an almost uniform distribution on the whole sphere.

Figure 6 shows two characteristic laser curves plotting continuous wave (CW) fiber coupled signal output power vs absorbed pump power (i.e., the difference between the launched and the residual power in the fiber after coupling). Figure 6a plots the lasing power at 1579 as a function of pump power at 980 nm for an Er^{3+}/Yb^{3+} doped tellurite glass bubble as the one shown in Fig. 2a. The red line represents a linear fit to the experimental data, from which a lasing threshold of 1.66 mW can be calculated [42]. Remarkably, laser emission wavelength tuning can be obtained not only by increasing pump power (which also affects the cavity temperature), but also changing the bubble internal pressure obtaining a tunability of − 6.6 GHz/bar. Figure 6b shows lasing power

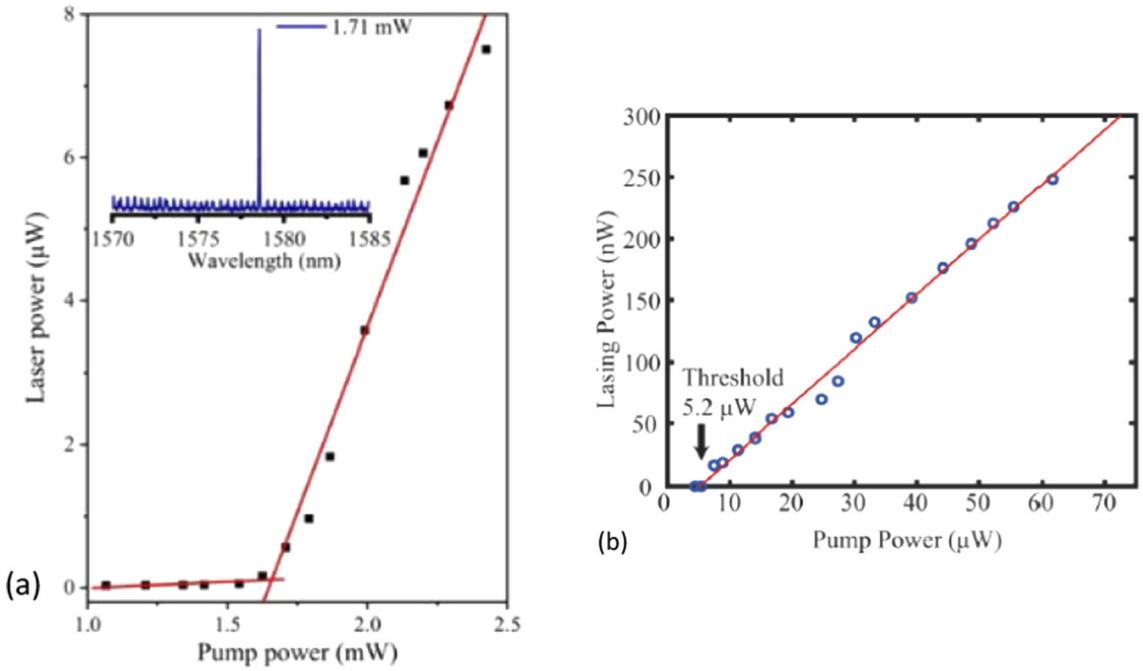

Fig. 6 **a** Characteristic curve showing lasing power at 1579 nm as a function of pump power at 980 nm for an Er^{3+}/Yb^{3+} doped tellurite glass bubble as the one shown in Fig. 2a. The red line represents a linear fit to the experimental data, with a lasing threshold of 1.66 mW. The inset is the output laser spectrum when the pump power is 1.71 mW (from [42]) and **b** characteristic curve showing lasing power at 1046 nm versus pump power at 973 nm for a Yb^{3+} silica microsphere fabricated on a silicon chip as the one shown in Fig. 2b (from [65]); a lasing threshold of around 5.2 μW is obtained through linear fitting (red curve)

at 1046 nm versus pump power at 973 nm for a Yb^{3+} silica microsphere on a chip as the one shown in Fig. 2b. The mechanism of the 1040 nm lasers involves transition of Yb^{3+} ions from $^2F_{5/2}$ to $^2F_{7/2}$ levels. Compared to the monolithic microbubble, the smaller on chip microsphere has a much lower lasing threshold of 5.2 μW [65].

Table 1 presents an exhaustive list of relevant contributions in the literature on glass WGM lasers from the early works in the mid-90's till today. The table lists the most significant information available in each manuscript, including lasing wavelength, peak power, pump wavelength and pump threshold (typically the 'absorbed' pump threshold rather than the launched one), WGM resonator type and size (in brackets the size of the 'demo' resonator, on which the main tests were performed), and coupling tool. We then indicate the RE dopant (and the possible co-doping), the glass type (typically a monolithic glass resonator, otherwise an active coating deposited on a passive resonator and having a thickness from few hundreds nanometers to few microns) and its composition, and finally the measured cold cavity Q factor.

4 Applications in sensing

Sensing with optical WGM resonators is based on monitoring the change of their spectral characteristics induced by a perturbation happening within the WGM spatial extension, including the resonator surface and the region immediately surrounding it, where the WGM evanescent tail still extends. This change can be either the broadening of the resonances (with Q factor reduction) due to additional losses, or, more typically, the shift of the resonance frequencies due a refractive index change [14, 133]. Considering that the ability to detect a shift is directly proportional to the resonant linewidth, the strong narrowing (up to a few order of magnitude [134]) of the laser line compared to the cold cavity resonance linewidth translates into a corresponding significant improvement of the transducer sensitivity [18, 19]. More generally, the analysis of the relative intensity noise (RIN) level of the micro-laser source becomes important as RIN may limit the sensor sensitivity. In Ref. [72] we presented an approach that could be extended to WGM laser frequency noise and exploited in the analysis of the whole noise properties of micro-lasers used in sensor applications.

In case biosensing like DNA hybridization is performed on the resonator while it is lasing, care should be taken to avoid reaching temperature that can destabilize DNA. Indeed, depending on the RE ions and the glass matrix, non-radiative transitions can be quite effective [135] increasing the temperature up to melting the glass [84, 101].

Another sensing mechanism is based on mode splitting of a very high-Q resonance due to nanoparticles at the resonator surfaces that couple the clockwise (CW) mode with the counterclockwise modes (CCW), thus lifting the degeneracy of the two modes [136]. The frequency splitting of an ultranarrow emission line of a WGM microlaser in two lines that move apart can be resolved and

Table 1 Summary of specifications of glass WGM lasers taken from the literature (1995–2022)

Lambda emission (nm)	Peak power (efficiency)	Pump wavelength (nm)	Pump threshold (absorbed power)/(efficiency)	Geometry	Diameter (μm) (demo)	Coupling system	Dopant	Glass type/ composition	Cold Q-factor	Year Biblio
860–865	N/A	514.5	N/A	Sphere	80–120	Microscope/free space	Nd^{3+}	N/A	N/A	1995 [20]
1060–1090	150 pW	810	200 nW	Sphere	50–80 (56)	Prism	Nd^{3+} (0.2% wt)	Silica	10^6	1996 [21]
1051 and 1334	N/A	800	5–60 mW	Sphere	140–150	Microscope/free space	Nd^{3+} (2% mol)	Fluoride (ZBLAN, $53ZrF_4$-$20BaF_2$-$2LaF_3$-$3AlF_3$-$20NaF$-$2NdF_3$, mol %)	N/A	1997 [29]
1048–1050	70 nW	806	100 μW (launched)	Sphere	112	Prism	Nd^{3+} (2000 ppmw)	Fluoride (ZBLAN)	N/A	1998 [49]
1060–1080	N/A	807	200 nW	Sphere	40–300	Prism	Nd^{3+} (0.2% wt)	Silica	N/A	1999 [85]
1560	N/A	1480	<600 μW	Sphere	10–200 (57)	Prism	Er^{3+}	Fluoride (ZBLAN)	N/A	1999 [25]
480 and 800 (upconversion)	N/A	1064 pulsed	20 mW/5 mW	Sphere	10–100 (65)	Microscope/free space	Tm^{3+} (1% mol)	Fluoride (ZBLAN: $53ZrF_4$, $20BaF_2$, $4LaF_3$, $3AlF_3$, and 20NaF: mol %)	N/A	1999 [27]
539 nm (upconversion)	N/A	801	30 μW	Sphere	60–120 (120)	Prism	Er^{3+}	Fluoride (ZBLAN)	N/A	1999 [86]
527–547 nm (upconversion)	N/A	801	30 μW	Sphere	60–120 (120)	prism	Er^{3+} (800 ppm)	Fluoride (ZBLAN)	N/A	2000 [17]
1530–1560	3 μW	977.6	N/A	Sphere	50–150	Angled-polished fiber	Er^{3+}	N/A	10^6	2000 [36]

Table 1 continued

Lambda emission (nm)	Peak power (efficiency)	Pump wavelength (nm)	Pump threshold (absorbed power)/(efficiency)	Geometry	Diameter (μm) (demo)	Coupling system	Dopant	Glass type/ composition	Cold Q-factor	Year Biblio
1560	N/A	1480	<600 μW	Sphere	56	Prism	Er^{3+} (0.2% wt)	Fluoride (ZBLAN)	N/A	2000 [87]
1530–1560	3 μW	980	60 μW	Sphere	50-few hundreds (57)	Fiber taper	Er^{3+} (0.5% wt)/Yb^{3+} (20% wt)	Phosphate (Kigre QX/Er)	N/A	2000 [26]
590–615	N/A	488	3.6 mW	Sphere	23	Prism (not matched)	Sm^{3+} (Sm_2O_3, 2% mol)	Borosilicate ($70SiO_2$, $15B_2O_3$, $15Na_2O$: mol %)	N/A	2001 [88]
1540–1600	140 nW	1480	600 μW	Sphere	50–95 (53)	Fiber taper/half taper	Er^{3+} (0.2% wt)	Fluoride (ZBLAN)	N/A	2001 [82]
1550	112 μW	980	400 μW	Sphere	45	Fiber taper (optimized)	Er^{3+}/Yb^{3+}	Phosphate	N/A	2001 [71]
1061–1067	N/A	800	81 mW	Sphere	50-few hundreds (140, 201)	Microscope/free space	Nd^{3+} (Nd_2O_3, 1% wt)	Tellurite ($70TeO_2$-$20ZnO$-$10Li_2O$, wt %)	N/A	2002 [28]
1556–1610 (1604)	<1 μW	975	<2 mW	sphere	33	Fiber taper	Er^{3+} (1.7×10^{20} ions/cm^3)	Tellurite	10^5–10^6	2003 [51]
1.535	10 μW	980	28 μW	Sphere (sol–gel coated)	50–80	Fiber taper	Er^{3+}	Silica (sol–gel coating)	N/A	2003 [53]
1550	2.6 μW	980	34 μW (11%)	Toroid on chip (sol–gel coated)	60–85	Fiber taper	Er^{3+} (~10^{19} ions/cm^3)	Silica (sol–gel coating)	N/A	2003 [54]
1606–1608 (1606)	41 μW	1480	2 mW	Sphere	32	Fiber taper	Er^{3+} (1.7×10^{20} ions/cm^3)	Tellurite	N/A	2003 [89]
1560–1600 (1576)	70 nW	1480	N/A	Sphere	10–200 (70)	Half taper	Er^{3+}/Yb^{3+} (Er_2O_3, 2% wt; Yb_2O_3, 3% wt)	Phosphate (Schott IOG-2)	N/A	2004 [90]

Table 1 continued

Lambda emission (nm)	Peak power (efficiency)	Pump wavelength (nm)	Pump threshold (absorbed power)/(efficiency)	Geometry	Diameter (μm) (demo)	Coupling system	Dopant	Glass type/ composition	Cold Q-factor	Year Biblio
1557–1589	39.4 μm	1472	4.5 μm (5.5%)	Toroid (on a chip)	25–80 (50)	Fiber taper	Er^{3+} ($0.6/6 \times 10^{19}$ ions/cm^3	Silica (Er^{3+} ions implanted)	3.9×10^7	2004 [23, 59]
1460–1530 & 1900 (1500)	350 nW	800	4.6 mW	Sphere	104	Fiber taper	Tm^{3+}, (0.15% Tm_2O_3)	Tellurite ($74.85TeO_2$-20ZnO-$5Na_2O$-$0.15Tm_2O_3$, wt %)	N/A	2004 [91]
1553	<1 μW	1480	660 nW	Toroid (on chip)	50–60	Fiber taper	Er^{3+} (2×10^{19} ions/cm^3)	Silica (sol–gel film)	$0.5/1 \times 10^7$	2005 [92]
1550–1610	124.5 μW	975	1.4 mW	Sphere	32	Fiber taper	Er^{3+} (Er_2O_3, 0.5% wt)	Tellurite	N/A	2005 [93]
635–680	N/A	400 (pulsed)	12–670 μW	Sphere (NC film coated)	6–20	Microscope/free space	CdSe/CdZnS nanocrystals	Titania (coating)	N/A	2005 [94]
1570–1610	300 μW	976	2 mW	Sphere (sol–gel coated)	40–200	Fiber taper	Er^{3+} (1250 to 15 000 ppm)	Alumino-silicate (89 SiO_2-$11Al_2O_3$, mol %) (sol–gel coating and bulk)	N/A	2005 [95]
1568	0.8 nW	1480	15 mW (launched)	Sphere	50–100 (80)	Half taper	Er^{3+} (0.2, 0.5, 1.5 mol%)	'Modified' silica (Baccarat)	N/A	2005 [96]
2000	21 μW	793	20 mW	Sphere	25	Fiber taper	Tm^{3+}, 0.2–9% wt	Tellurite	N/A	2005 [97]
1500 &1900	N/A	793	0.7 mW	Sphere	Tens to hundreds	Fiber taper	Tm^{3+} (Tm_2O_3 0.5% wt)	Tellurite	N/A	2005 [98]
1550–1600	40 nW	1450	150–250 μW (0.01%)	Sphere	44	Fiber taper	Er^{3+} (0.12–0.16% at.)	Silica	1.9×10^7	2006 [60]

Table 1 continued

Lambda emission (nm)	Peak power (efficiency)	Pump wavelength (nm)	Pump threshold (absorbed power)/(efficiency)	Geometry	Diameter (μm) (demo)	Coupling system	Dopant	Glass type/ composition	Cold Q-factor	Year Biblio
1510–1610	450 μW	976	0.3 mW	Sphere	40–150	Half taper	Er^{3+} (0.125–0.65% mol)	Alumino-silicate (bulk sol–gel)	$>10^8$	2006 [79]
1541–1569	120 nW	1480	2.5 mW (launched)	Sphere	85	Fiber taper/half taper	Er^{3+} (0.2, 0.5, 1.5% mol)	'Modified' silica (Baccarat)	N/A	2006 [81]
1555	10 μW	1480	43 μm	Disk (on chip)	60	Fiber taper	Er^{3+} 3.8×10^{20} ions/cm^3	Silica (Er^{3+} ions implanted)	5×10^7	2006 [22]
1560	30 nW	975	180 μW (launched)	Sphere (sol–gel coated)	40–200 (38)	Fiber taper	Er^{3+} (10,000 ppm)	Alumino-phosphate-silicate (sol–gel submicron coating)	N/A	2007 [99]
1042	12 μW	970	1.8 μW	Toroid (on chip)	40	Fiber taper	Yb^{3+} (4×10^{18} ions/cm^3)	Silica (sol–gel film)	2.5×10^7	2007 [44]
1527–1535	N/A	975	0.78 mW	Sphere (sol–gel coated)	40–45	Fiber taper	Er^{3+} (10,000 ppm)	Alumino-phosphate-silicate (sol–gel multilayer)	N/A	2008 [100]
1032 & 1563	15 μW	977	32 μW and 30 μW	Sphere	57	Fiber taper	Er^{3+} (1.25% mol)/Yb^{3+} (2.35% mol)	Phosphate glass	N/A	2008 [58]
1565	4.5 μW	977	N/A	Sphere	10–200	Fiber taper fused with μsphere	Er^{3+}/Yb^{3+} (Er_2O_3, 2% wt; Yb_2O_3, 3% wt)	Phosphate (Schott IOG-2 glass)	N/A	2008 [101]
510–560 (upconversion)	N/A (MM)	1458	690 μW	Toroid (on chip)	40	Fiber taper	Er^{3+} (0.1–0.5 at.%)	Silica (sol–gel film)	$>10^7$	2009 [102]
1520–1570	0.4 μW	980	4.2 μW	Toroid (on chip)	40	Fiber taper	Er^{3+} (0.05% wt)/Yb^{3+} (0.075% wt)	Silica (sol–gel film)	1×10^7	2009 [103]

Table 1 continued

Lambda emission (nm)	Peak power (efficiency)	Pump wavelength (nm)	Pump threshold (absorbed power)/(efficiency)	Geometry	Diameter (μm) (demo)	Coupling system	Dopant	Glass type/ composition	Cold Q-factor	Year Biblio
550 (upconversion)	N/A	978	3 μW	Sphere	30–120 (60)	Fiber taper	Er^{3+} (1.8% mol)	Fluorozirconate (ZBNA)	N/A	2010 [104]
1553 nm + 6 nm (tunable)	N/A	978	N/A	Sphere	50	Fiber taper	Er^{3+} /Yb^{3+} (Er_2O_3, 3% wt; Yb_2O_3, 5% wt)	Phosphate (Schott IOG-2 glass)	$>10^5$	2010 [105]
1088	15 nW	804	65 nW 7%	Sphere	41	Fiber taper	Nd^{3+}:Gd_2O_3 nanocrystals	Silica (activated surface)	1.4×10^8	2010 [80]
1075–1086	6 nW	808	N/A	Sphere	30–300	Microscope/free space	Nd^{3+} ($Nd_2(SO_4)_3$, 1.5% mol)	Chalcogenide (sulfide)	10^4–10^5	2010 [106]
1530–1610	3 nW	780	700 μW	Sphere (glass on glass coating)	40	Fiber taper	Er^{3+} (1.25% mol)	Phosphate	8×10^6	2010 [107]
1058–1068	100 nW	801	16 mW	Sphere	55	Integrated glass waveguide	Nd^{3+} (Nd_2O_3, 1.5% wt)	Borosilicate (BK7)	6×10^4	2011 [108]
1060–1070	N/A	810	14.5 mW	Sphere (air-bubble-containing or solid)	20–50 (40)	Microscope/free space	Nd^{3+} (Nd_2O_3, 1% mol)	Tellurite ($80TeO_2$-$10K_2O$-$10WO_3$, mol%)	N/A	2012 [109]
1900–2000	300 μW (SM), 800 μW (MM)	1611–1619	50 μW	Sphere	50–200 (75)	Fiber taper	Tm^{3+} (0.3 mol%)	Silica	10^4	2013 [110]
1598	130 nW	1480	4.8 μW	Sphere (on chip)	37	Fiber taper	Er^{3+} (2×10^{19} ions/cm^3)	Silica (sol–gel film)	1.6×10^6	2013 [111]
900, 1050–1130	N/A	780	0.53 μW (0.1%)	Toroid (on chip)	40	Fiber taper	Nd^{3+} (0.1 mol%)	Silica with alumina (2 mol%) (sol–gel film)	1.17×10^6	2013 [112]
1050–1130	25 μW	976	2.62 μW	Sphere (sol–gel coated)	60–130 (83)	Fiber taper	Yb^{3+} (1×10^{20} ions/cm^3)	Silica (sol–gel coating)	10^6	2014 [113]
2710	N/A	980	150 μW	Sphere	180	Fiber taper	Er^{3+} (8 mol%)	Fluoride (ZBLAN)	$>10^6$	2014 [114]

Table 1 continued

Lambda emission (nm)	Peak power (efficiency)	Pump wavelength (nm)	Pump threshold (absorbed power)/(efficiency)	Geometry	Diameter (μm) (demo)	Coupling system	Dopant	Glass type/ composition	Cold Q-factor	Year Biblio
1060–1070	N/A	800–810	0.6–2.4 mW	Sphere (terrace)	29	Microscope /free space	Nd^{3+}, (1 mol% Nd_2O_3)	Tellurite ($80TeO_2$-$10K_2O$-$10WO_3$, mol%)	N/A	2015 [77]
1975	800 nW	1504–1629	8.6–25 μW	Sphere	30	Fiber taper	Tm^{3+} (4.2×10^{20} cm^{-3})	Tellurite ($74TeO_2$-$15ZnO$-$5Na_2O$-$5ZnCl_2$-$1Tm_2O_3$, mol. %)	$>10^6$	2015 [115]
1.568	90 μW	1480 nm	< 1 mW	Sphere	75	Fiber taper	Er^{3+}/Yb^{3+}	Phosphate (Schott IOG-2)	0.8×10^6	2016 [32]
1535	N/A	980	3.6 mW (launched)	Bottle (tunable)	22–232	Fiber taper	Er^{3+}/Yb^{3+}	Phosphate	N/A	2016 [24]
1536	50 nW	980	27 mW	Bubble (tunable)	141	Fiber taper	Er^{3+} ($<5 \times 10^{19}$ ions/cm^3)	Silica (sol–gel drop on capillary)	10^6	2017 [55]
1100 & 905	30 nW and 125 nW	780	1.2 μW and 2.4 μW	Sphere (on chip)	36–42	Fiber taper	Nd^{3+} ($2.3–5.7 \times 10^{19}$ ions/cm^3)	Silica (sol–gel film)	N/A	2017 [45]
1976–2013	7.5 μW	808	3.1 mW	Sphere (sol–gel coated)	110–190	Fiber taper	Ho^{3+}:Tm^{3+} (Tm^{3+} 2–6 wt %, ratio 1/10)	Silica (sol–gel coating)	N/A	2017 [116]
2090–2100	110 nW	808	0.89 mW	Sphere	30–150 (60)	Fiber taper	Tm^{3+}/Ho^{3+} (Tm_2O_3, 1.0%; Ho_2O_3, 0.7%)	Tellurite ($75TeO_2$-$18.3ZnO$-$5Na_2O$-$1.0Tm_2O_3$-$0.7Ho_2O_3$)	5.34×10^6 @ 1550 nm	2017 [117]
1305.8	3.56 μW	808	215 μW	Sphere	50	Fiber taper	Bi_2O_3 (3.5 mol%)	Germanate ($70GeO_2$-$15Ga_2O_3$-$11.5BaO$-$3.5Bi_2O_3$, mol%)	2.5×10^5	2017 [118]
1060	N/A	805	0.6 mW	Sphere (terrace)	4–800 (29)	Free space	Nd^{3+} or Yb^{3+}	Tellurite	N/A	2018 [78]

Table 1 continued

Lambda emission (nm)	Peak power (efficiency)	Pump wavelength (nm)	Pump threshold (absorbed power)/(efficiency)	Geometry	Diameter (μm) (demo)	Coupling system	Dopant	Glass type/ composition	Cold Q-factor	Year Biblio
2004–2016, 2041	0.14 μW	980	14.7 mW	Sphere (sol–gel coated)	40–160	Fiber taper	Yb^{3+}(1.0 mol%)-Ho^{3+} (0.2 mol%)	Silica (sol–gel coating)	N/A	2018 [119]
545 (upconversion)	N/A	980	52.5 μW	Sphere	50–150 (58)	Fiber taper	Yb^{3+} (YbF_3 1.5 mol%)-Er^{3+} (Er_2O_3 0.1–0.5)	Fluorosilicate ($70SiO_2$-15KF-$15ZnF_2$, mol%)	N/A	2018 [120]
1535	100 nW	980	1.65 mW	Bottle (optically tunable)	121	Fiber taper	Er^{3+} (2×10^{19} ions/cm^3)	Silica (sol–gel coating)	5.2×10^7	2018 [56]
1850–2100	28 μW	808	1.2 mW	Sphere (sol–gel coated)	40–200	Fiber taper	Tm^{3+} (0.05–1.5 mol%)	Silica (sol–gel coating)	N/A	2018 [121]
1555–1565	0.6 μW	1480	N/A	Sphere (sol–gel coated)	130–300	Half taper	Er^{3+} (0.3 mol%)	Silica hafnia ($70SiO_2$-$30HfO_2$) (sol–gel coating)	N/A	2019 [122]
1495	114 nW	802	1.5 mW	Sphere	100	Fiber taper	Tm^{3+}/Ho^{3+} (Tm_2O_3 0.2%; Ho_2O_3 0.8%)	Tellurite ($72TeO_2$-$20ZnO$-$5.0Na_2CO_3$-$2.0Y_2O_3$-$0.8Ho_2O_3$-$0.2Tm_2O_3$)	N/A	2019 [123]
1891–1897	200 nW	ASE source (1527–1603 nm)	1.5 mW	Sphere	110	Fiber taper r	Er^{3+}/Tm^{3+} (Er_2O_3, 0.1%; Tm_2O_3, 0.2%)	Tellurite ($68.7TeO_2$-$23WO_3$-$8La_2O_3$-$0.1Er_2O_3$-$0.2Tm_2O_3$, mol%)	N/A	2019 [124]
2000–2040 (2023)	200 nW	1150	3.4 mW	Sphere (sol–gel coated)	114	Fiber taper	Ho^{3+}	Silica (sol–gel coating)	0.77×10^5	2019 [125]

Table 1 continued

Lambda emission (nm)	Peak power (efficiency)	Pump wavelength (nm)	Pump threshold (absorbed power)/(efficiency)	Geometry	Diameter (μm) (demo)	Coupling system	Dopant	Glass type/ composition	Cold Q-factor	Year Biblio
1880–1900 (1898)	90 nW	808	4.5 mW	Sphere	63	Fiber taper	Tm^{3+} (TmF_3, 1 mol%)	Fluoride (ZBYA, $50ZrF_4$-$33BaF_2$-$9YF_3$-$7AlF_3$-$1TmF_3$, mol%)	N/A	2019 [126]
1495–1570	1.4 μW	1480	21.2 μW	Sphere (from etched fiber)	60	Fiber taper	Er^{3+} (4000 ppm)	EDFL-980-HP, Nufern fiber	3×10^7	2019 [37]
1880	1 μW	808	5 mW	Sphere	52	Fiber taper	Tm^{3+} (0.3–1 mol%)	Fluorosilicate ($70SiO_2$-$15KF$-$15ZnF_2$, mol%)	1.4×10^6	2020 [127]
2065–2072	23 nW	980	1.4 mW	Sphere	80	Fiber taper	Ho^{3+}/Yb^{3+} (Ho_2O_3 0.2%/Yb_2O_3, 0.8%)	Tellurite ($72TeO_2$-$20ZnO$-$5Na_2CO_3$-$2Y_2O_3$-$0.8Yb_2O_3$-$0.2Ho_2O_3$)	10^5	2020 [128]
2080	1.1 μW	1150	324 μW	Sphere	42	Fiber taper	Ho^{3+} (HoF_3, 1% mol)	Tellurite ($72TeO_2$-$20ZnO$-$5Na_2CO_3$-$2Y_2O_3$-$1HoF_3$, mol%)	2×10^6	2020 [129]
1900–2080-2300	160 nW	793	7.4 mW, 0.3 mW, 5.0 mW	Sphere	60	Fiber taper	Tm^{3+}/Ho^{3+} (Tm_2O_3, 1%; Ho_2O_3, 0.2%)	Fluorotellurite ($70TeO_2$-$20BaF_2$-$8.8Y_2O_3$-$1Tm_2O_3$-$0.2Ho_2O_3$)	N/A	2020 [130]
1550	12 μW	980	1.66 mW	Bubble from tellurite capillary, (tunable)	132, 175	Fiber taper	Er^{3+}/Yb^{3+} ($0.5Yb_2O_3$-$0.25Er_2O_3$)	Tellurite ($75TeO_2$-$5ZnO$-$15Na_2CO_3$-$4.25Bi_2O_3$-$0.5Yb_2O_3$-$0.25Er_2O_3$	2.3×10^6	2020 [42]

Table 1 continued

Lambda emission (nm)	Peak power (efficiency)	Pump wavelength (nm)	Pump threshold (absorbed power)/(efficiency)	Geometry	Diameter (μm) (demo)	Coupling system	Dopant	Glass type/ composition	Cold Q-factor	Year Biblio
1026–1043	450 nW	970–980	5.2 μW–0.6 μW	Sphere (on chip)	19–21	Fiber taper	Yb^{3+} (4×10^{18} ions/cm^3)—Er^{3+}/Yb^{3+} ($1 \times 10^{19}/1 \times 10^{19}$ions/$cm^3$)	Silica (sol–gel film)	$0.8–3 \times 10^6$	2021 [65]
1595–1610	160 nW	ASE source (1000 nm)	N/A	Sphere (sol–gel coated)	80–220	Fiber taper	Er^{3+}/Yb^{3+}	Silica (sol–gel coating)	N/A	2021 [131]
537 (upconversion)	N/A	976	60 nW	Sphere (from etched fiber)	60–120 (100)	Fiber taper	Er^{3+} (0.6–0.8 at %)	Silica (coated with Al, Au and Pt metallic film)	N/A	2021 [132]
652, 545, 475 (white upconversion)	N/A	980 (pulsed)	~2 mJ/cm^2	Toroid (on chip)	86	Free space	CaF_2:$Yb_{35}Tm_{1.5}Er_{0.5}$ NCs	Silica (Lanthanide NC doped sol–gel film)	5×10^5	2022 [61]
380, 410, 450, 560, 660, 800 (upconversion), 1080, 1550	N/A	975	480, 170, 2.7, 18, 0.18, 1.7, 10, 38 μW	Sphere	57	Fiber taper	Er^{3+}/Yb^3	Silica (PMMA film assisted doped)	1.2×10^8	2022 [62]
1535	0.42 μW	980	16 μW (1%)	Sphere	600	Fiber taper	Er^{3+} ($>1 \times 10^{18}$ ions/cm^3)	Silica (liquid based surface doping) with graphene layer	8×10^7	2022 [64]

measured by recording their beat note. Indeed, this approach has been used with integrated Er^{3+} doped silica toroids to demonstrate single virus and nanoparticle detection [137]. Interestingly, we have shown that depending on the glass matrix the coupling between clockwise and counterclockwise modes has not the same strength, which strongly impacts the WGM laser dynamics [138].

Finally, a crucial advantage of using active WGM resonators as sensors is the fact that a free space architecture with remote excitation and readout can be implemented, as in the scheme sketched in Fig. 4b. After focusing the pump onto the resonator, the emission spectrum is collected with the same objective used for the excitation pump (or with a second one placed orthogonally [139]) and then sent to a spectrometer. This interrogation approach overcomes a critical restriction hindering the development of practical devices based on passive resonators where the light coupling scheme typically requires physical contact with the fiber taper or the prism (see Figs. 3 and 4a).

5 Conclusions

This work presents an extensive review of the literature on WGM micro-optical resonators made in rare-earth doped glasses. We first describe the fabrication techniques for making different types of monolithic spheroidal glass cavities, including those made on a chip, or those obtained depositing active glass layers on passive resonators. We then introduce the systems to couple the pump light into the cavities and collect the output signal in order to characterize the laser performances. An exhaustive table, listing all the relevant contributions in the literature on glass WGM lasers, represents the core of this work. From the early works in the mid-90's till today, more than 100 papers were reviewed and those presenting original contributions in any specification including pump threshold, emitting wavelength, RE dopant, glass composition, etc., were all listed in the table. Lasing wavelengths range from the visible (blue, 480 nm, and green, 540 nm) to the near infrared (from 800 nm up to 2300 nm), depending on the RE doping and the host glass. Pump lasing threshold below or of the order of tens of nanowatt (almost thresholdless) were measured when the pump was also resonant with a WGM. Because of their small size and ease of fabrication, these micro-laser sources can be a useful tool for the characterization of RE doped glasses. We finally identify the main application of these active cavities, which is that of optical transducer for sensing, listing their significant advantages compared to their passive counterparts.

Data Availability Statement No Data associated in the manuscript.

Declarations

Conflict of interest The authors have no conflict of interests or competing interests to declare that are relevant to the content of this article.

References

1. A. Chiasera, Y. Dumeige, P. Féron, M. Ferrari, Y. Jestin, G. Nunzi Conti, S. Pelli, S. Soria, G.C. Righini, Spherical whispering-gallery-mode microresonators. Laser Photonics Rev. **4**, 457–482 (2010). https://doi.org/10.1002/lpor.200910016
2. G.C. Righini, Y. Dumeige, P. Féron, G. Nunzi Conti, D. Ristic, S. Soria, Whispering gallery mode microresonators: fundamentals and applications. La Rivista del Nuovo Cimento. **34**, 435–488 (2011). https://doi.org/10.1393/ncr/i2011-10067-2
3. C.G.B. Garrett, W. Kaiser, W.L. Bond, Stimulated emission into optical whispering modes of spheres. Phys. Rev. **124**, 1807–1809 (1961). https://doi.org/10.1103/PhysRev.124.1807
4. H.-M. Tzeng, K.F. Wall, M.B. Long, R.K. Chang, Laser emission from individual droplets at wavelengths corresponding to morphology-dependent resonances. Opt. Lett. **9**, 499–501 (1984). https://doi.org/10.1364/OL.9.000499
5. M. Kuwata-Gonokami, K. Takeda, H.Y.H. Yasuda, K.E.K. Ema, Laser emission from dye-doped polystyrene microsphere. Jpn. J. Appl. Phys. **31**, L99 (1992). https://doi.org/10.1143/JJAP.31.L99
6. V.B. Braginsky, M.L. Gorodetsky, V.S. Ilchenko, Quality-factor and nonlinear properties of optical whispering-gallery modes. Phys. Lett. A **137**, 393–397 (1989). https://doi.org/10.1016/0375-9601(89)90912-2
7. J. Yu, E. Lewis, G. Farrell, P. Wang, Compound glass microsphere resonator devices. Micromachines. **9**, 356 (2018). https://doi.org/10.3390/mi9070356
8. S. Berneschi, F. Cosi, D. Farnesi, G. Frigenti, G.C. Righini, S. Pelli, S. Soria, F. Baldini, F. Prudenzano, G. Persichetti, R. Bernini, Y. Dumeige, P. Féron, D. Ristić, M. Ivanda, G. N. Conti, Glass based microresonators, in *Fiber Lasers and Glass Photonics: Materials through Applications* (SPIE, 2018), pp. 75–82
9. S.M. Spillane, T.J. Kippenberg, K.J. Vahala, Ultralow-threshold Raman laser using a spherical dielectric microcavity. Nature **415**, 621–623 (2002). https://doi.org/10.1038/415621a
10. D. Farnesi, A. Barucci, G.C. Righini, S. Berneschi, S. Soria, G. Nunzi Conti, Optical frequency conversion in silica-whispering-gallery-mode microspherical resonators. Phys. Rev. Lett. **112**, 093901 (2014). https://doi.org/10.1103/PhysRevLett.112.093901
11. E. Kim, M.D. Baaske, F. Vollmer, Towards next-generation label-free biosensors: recent advances in whispering gallery mode sensors. Lab Chip. **17**, 1190–1205 (2017). https://doi.org/10.1039/C6LC01595F
12. B.J. Thompson, A.B. Matsko, *Practical Applications of Microresonators in Optics and Photonics* (CRC Press, Boca Raton, 2019)

13. G.C. Righini, Glass Micro- and Nanospheres: Physics and Applications. https://www.routledge.com/Glass-Micro–and-Nanospheres-Physics-and-Applications/Righini/p/book/9789814774635
14. X. Jiang, A.J. Qavi, S.H. Huang, L. Yang, Whispering-gallery sensors. Matter **3**, 371–392 (2020). https://doi.org/10.1016/j.matt.2020.07.008
15. L. He, ŞK. Özdemir, L. Yang, Whispering gallery microcavity lasers. Laser Photonics Rev. **7**, 60–82 (2013). https://doi.org/10.1002/lpor.201100032
16. E.A. Anashkina, Laser sources based on rare-earth ion doped tellurite glass fibers and microspheres. Fibers **8**, 30 (2020). https://doi.org/10.3390/fib8050030
17. W. von Klitzing, E. Jahier, R. Long, F. Lissillour, V. Lefèvre-Seguin, J. Hare, J.-M. Raimond, S. Haroche, Very low threshold green lasing in microspheres by up-conversion of IR photons. J. Opt. B Quantum Semiclass. Opt. **2**, 204–206 (2000). https://doi.org/10.1088/1464-4266/2/2/324
18. T. Reynolds, N. Riesen, A. Meldrum, X. Fan, J.M.M. Hall, T.M. Monro, A. François, Fluorescent and lasing whispering gallery mode microresonators for sensing applications. Laser Photonics Rev. **11**, 1600265 (2017). https://doi.org/10.1002/lpor.201600265
19. N. Toropov, G. Cabello, M.P. Serrano, R.R. Gutha, M. Rafti, F. Vollmer, Review of biosensing with whispering-gallery mode lasers. Light Sci. Appl. **10**, 42 (2021). https://doi.org/10.1038/s41377-021-00471-3
20. Y.Z. Wang, B.L. Lu, Y.Q. Li, Y.S. Liu, Observation of cavity quantum-electrodynamic effects in a Nd:glass microsphere. Opt. Lett. **20**, 770–772 (1995). https://doi.org/10.1364/OL.20.000770
21. V. Sandoghdar, F. Treussart, J. Hare, V. Lefèvre-Seguin, J.-M. Raimond, S. Haroche, Very low threshold whispering-gallery-mode microsphere laser. Phys. Rev. A **54**, R1777–R1780 (1996). https://doi.org/10.1103/PhysRevA.54.R1777
22. T.J. Kippenberg, J. Kalkman, A. Polman, K.J. Vahala, Demonstration of an erbium-doped microdisk laser on a silicon chip. Phys. Rev. A **74**, 051802 (2006). https://doi.org/10.1103/PhysRevA.74.051802
23. A. Polman, B. Min, J. Kalkman, T.J. Kippenberg, K.J. Vahala, Ultralow-threshold erbium-implanted toroidal microlaser on silicon. Appl. Phys. Lett. **84**, 1037–1039 (2004). https://doi.org/10.1063/1.1646748
24. J.M. Ward, Y. Yang, S. Nic Chormaic, Glass-on-glass fabrication of bottle-shaped tunable microlasers and their applications. Sci Rep. **6**, 25152 (2016). https://doi.org/10.1038/srep25152
25. F.Lissillour, P. Feron, N. Dubreuil, P. Dupriez, G.M. Stephan, M. Poulain, Whispering-gallery mode Er-ZBLAN microlasers at 1.56 um, in *Laser Resonators II* (SPIE, 1999), pp. 199–205
26. M. Cai, O. Painter, K.J. Vahala, P.C. Sercel, Fiber-coupled microsphere laser. Opt. Lett. **25**, 1430–1432 (2000). https://doi.org/10.1364/OL.25.001430
27. H. Fujiwara, K. Sasaki, Upconversion lasing of a thulium-ion-doped fluorozirconate glass microsphere. J. Appl. Phys. **86**, 2385–2388 (1999). https://doi.org/10.1063/1.371064
28. K. Sasagawa, K. Kusawake, J. Ohta, M. Nunoshita, Nd-doped tellurite glass microsphere laser. Electron. Lett. **38**, 1355–1357 (2002)
29. K. Miura, K. Tanaka, K. Hirao, CW laser oscillation on both the $^4F_{3/2}$–$^4I_{11/2}$ and $^4F_{3/2}$–$^4I_{13/2}$ transitions of Nd^{3+} ions using a fluoride glass microsphere. J. Non-Cryst. Solids **213–214**, 276–280 (1997). https://doi.org/10.1016/S0022-3093(96)00671-0
30. A.A. Savchenkov, A.B. Matsko, V.S. Ilchenko, L. Maleki, Optical resonators with ten million finesse. Opt. Express **15**, 6768–6773 (2007). https://doi.org/10.1364/OE.15.006768
31. A.E. Shitikov, I.A. Bilenko, N.M. Kondratiev, V.E. Lobanov, A. Markosyan, M.L. Gorodetsky, Billion Q-factor in silicon WGM resonators. Optica **5**, 1525–1528 (2018). https://doi.org/10.1364/OPTICA.5.001525
32. D. Ristić, S. Berneschi, M. Camerini, D. Farnesi, S. Pelli, C. Trono, A. Chiappini, A. Chiasera, M. Ferrari, A. Lukowiak, Y. Dumeige, P. Féron, G.C. Righini, S. Soria, G.N. Conti, Photoluminescence and lasing in whispering gallery mode glass microspherical resonators. J. Lumin. **170**, 755–760 (2016). https://doi.org/10.1016/j.jlumin.2015.10.050
33. L. Collot, V. Lefèvre-Seguin, M. Brune, J.M. Raimond, S. Haroche, Very high-Q whispering-gallery mode resonances observed on fused silica microspheres. EPL **23**, 327–334 (1993). https://doi.org/10.1209/0295-5075/23/5/005
34. K.-C. Fan, H.-Y. Hsu, P.-Y. Hung, W. Wang, Experimental study of fabricating a microball tip on an optical fibre. J. Opt. A Pure Appl. Opt. **8**, 782–787 (2006). https://doi.org/10.1088/1464-4258/8/9/012
35. P. Wang, G.S. Murugan, T. Lee, X. Feng, Y. Semenova, Q. Wu, W. Loh, G. Brambilla, J.S. Wilkinson, G. Farrell, Lead silicate glass microsphere resonators with absorption-limited Q. Appl. Phys. Lett. (2011). https://doi.org/10.1063/1.3586771
36. V.S. Ilchenko, X.S. Yao, L. Maleki, Microsphere integration in active and passive photonics devices. Presentato al Symposium on High-Power Lasers and Applications, San Jose, CA maggio 12 (2000)
37. Z. Chen, X. Tu, J. Zhao, H.Y. Fu, An erbium-doped fiber whispering-gallery-mode microcavity laser. IEEE Photonics Technol. Lett. **31**, 1650–1653 (2019). https://doi.org/10.1109/LPT.2019.2942046
38. M. Sumetsky, Lasing microbottles. Light Sci. Appl. **6**, e17102 (2017). https://doi.org/10.1038/lsa.2017.102
39. G.S. Murugan, J.S. Wilkinson, M.N. Zervas, Selective excitation of whispering gallery modes in a novel bottle microresonator. Opt. Express **17**, 11916–11925 (2009). https://doi.org/10.1364/OE.17.011916
40. S.B. Gorajoobi, G.S. Murugan, M.N. Zervas, Mode-selective spectrally-cleaned-up microbottle resonator laser, in *2016 IEEE Photonics Conference (IPC)* (2016), pp. 105–106
41. S.B. Gorajoobi, G.S. Murugan, M.N. Zervas, Design of rare-earth-doped microbottle lasers. Opt. Express **26**, 26339–26354 (2018). https://doi.org/10.1364/OE.26.026339
42. J. Yu, J. Yu, J. Zhang, R. Wang, A. Li, A. Li, M. Zhang, S. Wang, P. Wang, P. Wang, P. Wang, J.M. Ward, J.M. Ward, S.N. Chormaic, S.N. Chormaic, A tellurite glass optical microbubble resonator. Opt. Express **28**, 32858–32868 (2020). https://doi.org/10.1364/OE.406256
43. A. Chiappini, A. Chiasera, S. Berneschi, C. Armellini, A. Carpentiero, M. Mazzola, E. Moser, S. Varas, G.C. Righini, M. Ferrari, Sol–gel-derived photonic structures: fabrication, assessment, and application. J. Sol-Gel Sci. Technol. **60**, 408–425 (2011). https://doi.org/10.1007/s10971-011-2556-y
44. E.P. Ostby, L. Yang, K.J. Vahala, Ultralow-threshold Yb^{3+}:SiO_2 glass laser fabricated by the solgel process. Opt. Lett. **32**, 2650–2652 (2007). https://doi.org/10.1364/OL.32.002650
45. Y. Ding, H. Fan, X. Zhang, X. Jiang, M. Xiao, Ultralow-threshold neodymium-doped microsphere lasers on a silicon chip. Opt. Commun. **395**, 51–54 (2017). https://doi.org/10.1016/j.optcom.2016.01.028
46. J. Lin, Y. Xu, J. Song, B. Zeng, F. He, H. Xu, K. Sugioka, W. Fang, Y. Cheng, Low-threshold whispering-gallery-mode microlasers fabricated in a Nd:glass substrate by three-dimensional femtosecond laser micromachining. Opt. Lett. **38**, 1458–1460 (2013). https://doi.org/10.1364/OL.38.001458
47. G.N. Conti, A. Barucci, S. Berneschi, M. Brenci, F. Cosi, D. Farnesi, S. Pelli, G.C. Righini, S. Soria, Coupling approaches and new geometries in whispering-gallery-mode resonators, in *Laser Resonators, Microresonators, and Beam Control XIV* (SPIE, 2012), pp. 195–202
48. D. Farnesi, G.C. Righini, A. Barucci, S. Berneschi, F. Chiavaioli, F. Cosi, S. Pelli, S. Soria, C. Trono, D. Ristic, M. Ferrari, G.N. Conti, Coupling light to whispering gallery mode resonators, in *Silicon Photonics and Photonic Integrated Circuits IV* (SPIE, 2014), pp. 179–187
49. F. Lissillour, K.A. Ameur, N. Dubreuil, G.M. Stephan, M. Poulain, Whispering-gallery-mode Nd-ZBLAN microlasers at 1.05 um, in *Infrared Glass Optical Fibers and Their Applications* (SPIE, 1998), pp. 150–156

50. J.M. Ward, Y. Wu, K. Khalfi, S.N. Chormaic, Short vertical tube furnace for the fabrication of doped glass microsphere lasers. Rev. Sci. Instrum. **81**, 073106 (2010). https://doi.org/10.1063/1.3455198
51. X. Peng, F. Song, S. Jiang, N. Peyghambarian, M. Kuwata-Gonokami, L. Xu, Fiber-taper-coupled L-band Er^{3+}-doped tellurite glass microsphere laser. Appl. Phys. Lett. **82**, 1497–1499 (2003). https://doi.org/10.1063/1.1559653
52. G.C. Righini, C. Armellini, A. Chiasera, Y. Jestin, M. Ferrari, A. Chiappini, M. Montagna, C.A. Duverger, P. Féron, S. Berneschi, M. Brenci, G.N. Conti, S. Pelli, C. Gonçalves, R.M. Almeida, Er^{3+}-activated sol–gel silica derived spherical microresonators. Glass Technol. **48**, 4 (2006)
53. L. Yang, K.J. Vahala, Gain functionalization of silica microresonators. Opt. Lett. **28**, 592–594 (2003). https://doi.org/10.1364/OL.28.000592
54. L. Yang, D.K. Armani, K.J. Vahala, Fiber-coupled erbium microlasers on a chip. Appl. Phys. Lett. **83**, 825–826 (2003). https://doi.org/10.1063/1.1598623
55. Y. Yang, F. Lei, S. Kasumie, L. Xu, J.M. Ward, L. Yang, S.N. Chormaic, Tunable erbium-doped microbubble laser fabricated by sol–gel coating. Opt. Express **25**, 1308–1313 (2017). https://doi.org/10.1364/OE.25.001308
56. S. Zhu, L. Shi, B. Xiao, X. Zhang, X. Fan, All-optical tunable microlaser based on an ultrahigh-Q erbium-doped hybrid microbottle cavity. ACS Photonics **5**, 3794–3800 (2018). https://doi.org/10.1021/acsphotonics.8b00838
57. D. Ristić, A. Rasoloniaina, A. Chiappini, P. Féron, S. Pelli, G.N. Conti, M. Ivanda, G.C. Righini, G. Cibiel, M. Ferrari, About the role of phase matching between a coated microsphere and a tapered fiber: experimental study. Opt. Express **21**, 20954–20963 (2013). https://doi.org/10.1364/OE.21.020954
58. C.-H. Dong, Y.-F. Xiao, Z.-F. Han, G.-C. Guo, X. Jiang, L. Tong, C. Gu, H. Ming, Low-threshold microlaser in Er:Yb phosphate glass coated microsphere. IEEE Photonics Technol. Lett. **20**, 342–344 (2008). https://doi.org/10.1109/LPT.2007.915642
59. B. Min, T.J. Kippenberg, L. Yang, K.J. Vahala, J. Kalkman, A. Polman, Erbium-implanted high-Q silica toroidal microcavity laser on a silicon chip. Phys. Rev. A. **70**, 033803 (2004). https://doi.org/10.1103/PhysRevA.70.033803
60. J. Kalkman, A. Polman, T.J. Kippenberg, K.J. Vahala, M.L. Brongersma, Erbium-implanted silica microsphere laser. Nucl. Instrum. Methods Phys. Res. Sect. B **242**, 182–185 (2006). https://doi.org/10.1016/j.nimb.2005.08.160
61. L. Jin, L. Jin, Z. Liu, Y. Zhang, Y. Wu, Y. Liu, H. Deng, Q. Song, Q. Song, Q. Song, Q. Song, S. Xiao, S. Xiao, S. Xiao, S. Xiao, Lanthanide-doped nanocrystals in high-Q microtoroids for stable on-chip white-light lasers. Photonics Res. **10**, 1594–1601 (2022). https://doi.org/10.1364/PRJ.456381
62. B. Jiang, S. Zhu, L. Ren, L. Shi, X. Zhang, Simultaneous ultraviolet, visible, and near-infrared continuous-wave lasing in a rare-earth-doped microcavity. AP **4**, 046003 (2022). https://doi.org/10.1117/1.AP.4.4.046003
63. F. Kotz, K. Arnold, W. Bauer, D. Schild, N. Keller, K. Sachsenheimer, T.M. Nargang, C. Richter, D. Helmer, B.E. Rapp, Three-dimensional printing of transparent fused silica glass. Nature **544**, 337–339 (2017). https://doi.org/10.1038/nature22061
64. Y. Guo, Z. Li, N. An, Y. Guo, Y. Wang, Y. Yuan, H. Zhang, T. Tan, C. Wu, B. Peng, G. Soavi, Y. Rao, B. Yao, A monolithic graphene-functionalized microlaser for multispecies gas detection. Adv. Mater. (2022). https://doi.org/10.1002/adma.202207777
65. Y.-Q. Hu, X. Mao, H. Yang, M. Wang, G.-Q. Qin, G.-L. Long, Demonstration of Yb^{3+}-doped and Er^{3+}/Yb^{3+}-codoped on-chip microsphere lasers. Opt. Express **29**, 25663–25674 (2021). https://doi.org/10.1364/OE.427356
66. J.C. Knight, G. Cheung, F. Jacques, T.A. Birks, Phase-matched excitation of whispering-gallery-mode resonances by a fiber taper. Opt. Lett. **22**, 1129–1131 (1997). https://doi.org/10.1364/OL.22.001129
67. G.N. Conti, S. Berneschi, F. Cosi, S. Pelli, S. Soria, G.C. Righini, M. Dispenza, A. Secchi, Planar coupling to high-Q lithium niobate disk resonators. Opt. Express **19**, 3651–3656 (2011). https://doi.org/10.1364/OE.19.003651
68. A. Rasoloniaina, V. Huet, T.K.N. Nguyên, E. Le Cren, M. Mortier, L. Michely, Y. Dumeige, P. Féron, Controling the coupling properties of active ultrahigh-Q WGM microcavities from undercoupling to selective amplification. Sci. Rep. **4**, 4023 (2014). https://doi.org/10.1038/srep04023
69. K. Totsuka, M. Tomita, Optical microsphere amplification system. Opt. Lett. **32**, 3197–3199 (2007). https://doi.org/10.1364/OL.32.003197
70. A. Rasoloniaina, S. Trebaol, V. Huet, E.L. Cren, G.N. Conti, H. Serier-Brault, M. Mortier, Y. Dumeige, P. Féron, High-gain wavelength-selective amplification and cavity ring down spectroscopy in a fluoride glass erbium-doped microsphere. Opt. Lett. **37**, 4735–4737 (2012). https://doi.org/10.1364/OL.37.004735
71. M. Cai, K. Vahala, Highly efficient hybrid fiber taper coupled microsphere laser. Opt. Lett. **26**, 884–886 (2001). https://doi.org/10.1364/OL.26.000884
72. J.-B. Ceppe, M. Mortier, P. Féron, Y. Dumeige, Theoretical and experimental analysis of rare earth whispering gallery mode laser relative intensity noise. Opt. Express **25**, 32732–32744 (2017). https://doi.org/10.1364/OE.25.032732
73. L. Xiao, S. Trebaol, Y. Dumeige, Z. Cai, M. Mortier, P. Feron, Miniaturized optical microwave source using a dual-wavelength whispering gallery mode laser. IEEE Photonics Technol. Lett. **22**, 559–561 (2010). https://doi.org/10.1109/LPT.2010.2040269
74. A. Li, A. Li, K. Tian, J. Yu, J. Yu, R.A. Minz, J.M. Ward, S. Mondal, P. Wang, P. Wang, P. Wang, S.N. Chormaic, S.N. Chormaic, Packaged whispering gallery resonator device based on an optical nanoantenna coupler. Opt. Express **29**, 16879–16886 (2021). https://doi.org/10.1364/OE.422830
75. M.L. Gorodetsky, V.S. Ilchenko, Optical microsphere resonators: optimal coupling to high-Q whispering-gallery modes. J. Opt. Soc. Am. B **16**, 147–154 (1999). https://doi.org/10.1364/JOSAB.16.000147
76. X. Zambrana-Puyalto, D. D'Ambrosio, G. Gagliardi, Excitation mechanisms of whispering gallery modes with direct light scattering. Laser Photonics Rev. **15**, 2000528 (2021). https://doi.org/10.1002/lpor.202000528
77. T. Kishi, T. Kumagai, S. Shibuya, F. Prudenzano, T. Yano, S. Shibata, Quasi-single mode laser output from a terrace structure added on a Nd^{3+}-doped tellurite-glass microsphere prepared using localized laser heating. Opt. Express **23**, 20629–20635 (2015). https://doi.org/10.1364/OE.23.020629
78. T. Kishi, On-chip fabrication of micrometer-size super-hemispherical and spherical optical devices from molten glass droplets. J. Ceram. Soc. Jpn. **126**, 495–503 (2018). https://doi.org/10.2109/jcersj2.18030
79. L.N. Chung, C.T.T. Ha, N.T. Trang, P.T. Nga, P.V. Hoi, B.V. Thien, High-power microcavity lasers based on highly erbium-doped sol–gel aluminosilicate glasses. Mater. Sci. Eng. B **131**, 27–31 (2006). https://doi.org/10.1016/j.mseb.2005.12.033
80. G. Lin, O. Tillement, Y. Candela, M. Martini, Z. Cai, V. Lefèvre-Seguin, J. Hare, Ultra-low threshold lasing in silica whispering-gallery-mode microcavities with Nd^{3+}:Gd_2O_3 nanocrystals, in *Micro-Optics 2010* (SPIE, 2010), pp. 600–607
81. G. Nunzi Conti, A. Chiasera, L. Ghisa, S. Berneschi, M. Brenci, Y. Dumeige, S. Pelli, S. Sebastiani, P. Feron, M. Ferrari, G.C. Righini, Spectroscopic and lasing properties of Er^{3+}-doped glass microspheres. J. Non-Cryst. Solids **352**, 2360–2363 (2006). https://doi.org/10.1016/j.jnoncrysol.2006.01.089
82. F. Lissillour, D. Messager, G. Stéphan, P. Féron, Whispering-gallery-mode laser at 1.56 μm excited by a fiber taper. Opt. Lett. **26**, 1051–1053 (2001). https://doi.org/10.1364/OL.26.001051
83. C. Arnaud, M. Boustimi, M. Brenci, P. Feron, M. Ferrari, G. Nunzi-Conti, S. Pelli, G.C. Righini, Microsphere laser in Er^{3+}-doped oxide glasses, in *5th Iberoamerican Meeting on Optics and 8th Latin American Meeting on Optics, Lasers, and Their Applications* (SPIE, 2004), pp. 315–320
84. C. Pérez-Rodríguez, L. Labrador-Páez, I.R. Martín, S. Ríos, Temperature response of the whispering gallery mode resonances from the green upconversion emission of an Er^{3+}–Yb^{3+} co-doped microsphere. Laser Phys. Lett. **12**, 046003 (2015). https://doi.org/10.1088/1612-2011/12/4/046003
85. V. Lefèvre-Seguin, Whispering-gallery mode lasers with doped silica microspheres. Opt. Mater. **11**, 153–165 (1999). https://doi.org/10.1016/S0925-3467(98)00041-X

86. W. von Klitzing, E. Jahier, R. Long, F. Lissillour, V. Lefevre-Seguin, J. Hare, J.-M. Raimond, S. Haroche, Very low threshold lasing in Er^{3+} doped ZBLAN microsphere. Electron. Lett. **35**, 1745–1746 (1999). https://doi.org/10.1049/el:19991009
87. F. Lissillour, P. Féron, N. Dubreuil, P. Dupriez, M. Poulain, G.M. Stéphan, Erbium-doped microspherical lasers at 1.56 μm. Electron. Lett. **36**, 1382–1384 (2000). https://doi.org/10.1049/el:20001012
88. T. Hayakawa, H. Ooishi, M. Nogami, Optical bistability of stimulated-emission lines in Sm^{3+}-doped glass microspheres. Opt. Lett. **26**, 84–86 (2001). https://doi.org/10.1364/OL.26.000084
89. X. Peng, F. Song, M. Kuwata-Gonokami, S. Jiang, N. Peyghambarian, Temperature dependence of the wavelength and threshold of fiber-taper-coupled L-band Er^{3+}-doped tellurite glass microsphere laser. Appl. Phys. Lett. **83**, 5380–5382 (2003). https://doi.org/10.1063/1.1637454
90. C. Arnaud, M. Boustimi, P. Feron, G. Nunzi-Conti, G. Righini, Microsphere laser in Er^{3+}/Yb^{3+}-codoped phosphate glass: coupling with an external cavity, in *Laser Resonators and Beam Control VII* (SPIE, 2004), pp. 140–149
91. K. Sasagawa, Z. Yonezawa, R. Iwai, J. Ohta, M. Nunoshita, S-band Tm^{3+}-doped tellurite glass microsphere laser via a cascade process. Appl. Phys. Lett. **85**, 4325–4327 (2004). https://doi.org/10.1063/1.1810628
92. L. Yang, T. Carmon, B. Min, S.M. Spillane, K.J. Vahala, Erbium-doped and Raman microlasers on a silicon chip fabricated by the sol–gel process. Appl. Phys. Lett. **86**, 091114 (2005). https://doi.org/10.1063/1.1873043
93. X. Peng, F. Song, M.K. Gonokami, S. Jiang, N.N. Peyghambarian, Er^{3+}-doped tellurite glass microsphere laser: optical properties, coupling scheme, and lasing characteristics. Opt. Express. **44**, 034202 (2005). https://doi.org/10.1117/1.1869995
94. P.T. Snee, Y. Chan, D.G. Nocera, M.G. Bawendi, Whispering-gallery-mode lasing from a semiconductor nanocrystal/microsphere resonator composite. Adv. Mater. **17**, 1131–1136 (2005). https://doi.org/10.1002/adma.200401571
95. P. Van Hoi, C.T.T. Ha, H.Q. Hung, Long-band emission of microsphere lasers based on erbium-doped sol–gel silica-alumina glasses. Appl. Phys. Lett. **87**, 161110 (2005). https://doi.org/10.1063/1.2089186
96. G.C. Righini, C. Arnaud, S. Berneschi, M. Bettinelli, M. Brenci, A. Chiasera, P. Feron, M. Ferrari, M. Montagna, G. Nunzi Conti, S. Pelli, H. Portales, C. Siligardi, A. Speghini, L. Zampedri, Integrated optical amplifiers and microspherical lasers based on erbium-doped oxide glasses. Opt. Mater. **27**, 1711–1717 (2005). https://doi.org/10.1016/j.optmat.2004.11.041
97. J. Wu, S. Jiang, T. Qua, M. Kuwata-Gonokami, N. Peyghambarian, 2 μm lasing from highly thulium doped tellurite glass microsphere. Appl. Phys. Lett. **87**, 211118 (2005). https://doi.org/10.1063/1.2132532
98. J. Wu, S. Jiang, N. Peyghambarian, 15-μm-band thulium-doped microsphere laser originating from self-terminating transition. Opt. Express **13**, 10129–10133 (2005). https://doi.org/10.1364/OPEX.13.010129
99. H. Takashima, H. Fujiwara, S. Takeuchi, K. Sasaki, M. Takahashi, Fiber-microsphere laser with a submicrometer sol–gel silica glass layer codoped with erbium, aluminum, and phosphorus. Appl. Phys. Lett. **90**, 101103 (2007). https://doi.org/10.1063/1.2711384
100. H. Takashima, H. Fujiwara, S. Takeuchi, K. Sasaki, M. Takahashi, Control of spontaneous emission coupling factor β in fiber-coupled microsphere resonators. Appl. Phys. Lett. **92**, 071115 (2008). https://doi.org/10.1063/1.2884329
101. J.M. Ward, P. Feron, S. Nic Chormaic, A taper-fused microspherical laser source. IEEE Photonics Technol. Lett. **20**, 392–394 (2008). https://doi.org/10.1109/LPT.2008.916904
102. T. Lu, L. Yang, R.V.A. van Loon, A. Polman, K.J. Vahala, On-chip green silica upconversion microlaser. Opt. Lett. **34**, 482–484 (2009). https://doi.org/10.1364/OL.34.000482
103. H.-S. Hsu, C. Cai, A.M. Armani, Ultra-low-threshold Er:Yb sol–gel microlaser on silicon. Opt. Express **17**, 23265–23271 (2009). https://doi.org/10.1364/OE.17.023265
104. Y. Wu, J.M. Ward, S. Nic Chormaic, Ultralow threshold green lasing and optical bistability in ZBNA (ZrF_4–BaF_2–NaF–AlF_3) microspheres. J. Appl. Phys. **107**, 033103 (2010). https://doi.org/10.1063/1.3277024
105. J.M. Ward, S.N. Chormaic, Thermo-optical tuning of whispering gallery modes in Er:Yb co-doped phosphate glass microspheres. Appl. Phys. B **100**, 847–850 (2010). https://doi.org/10.1007/s00340-010-4153-0
106. G.R. Elliott, G.S. Murugan, J.S. Wilkinson, M.N. Zervas, D.W. Hewak, Chalcogenide glass microsphere laser. Opt. Express **18**, 26720–26727 (2010). https://doi.org/10.1364/OE.18.026720
107. C.H. Dong, Y. Yang, Y.L. Shen, C.L. Zou, F.W. Sun, H. Ming, G.C. Guo, Z.F. Han, Observation of microlaser with Er-doped phosphate glass coated microsphere pumped by 780nm. Opt. Commun. **283**, 5117–5120 (2010). https://doi.org/10.1016/j.optcom.2010.07.018
108. G.S. Murugan, M.N. Zervas, Y. Panitchob, J.S. Wilkinson, Integrated Nd-doped borosilicate glass microsphere laser. Opt. Lett. **36**, 73–75 (2011). https://doi.org/10.1364/OL.36.000073
109. T. Kishi, T. Kumagai, T. Yano, S. Shibata, On-chip fabrication of air-bubble-containing Nd^{3+}-doped tellurite glass microsphere for laser emission. AIP Adv. **2**, 042169 (2012). https://doi.org/10.1063/1.4769888
110. A. Pal, S.Y. Chen, R. Sen, T. Sun, K.T.V. Grattan, A high-Q low threshold thulium-doped silica microsphere laser in the 2 μm wavelength region designed for gas sensing applications. Laser Phys. Lett. **10**, 085101 (2013). https://doi.org/10.1088/1612-2011/10/8/085101
111. H. Fan, S. Hua, X. Jiang, M. Xiao, Demonstration of an erbium-doped microsphere laser on a silicon chip. Laser Phys. Lett. **10**, 105809 (2013). https://doi.org/10.1088/1612-2011/10/10/105809
112. A.J. Maker, A.M. Armani, Nanowatt threshold, alumina sensitized neodymium laser integrated on silicon. Opt. Express **21**, 27238–27245 (2013). https://doi.org/10.1364/OE.21.027238
113. Y. Huang, Y. Huang, P. Zhang, C. Guo, Ultralow-threshold laser and blue shift cooperative luminescence in a Yb^{3+} doped silica microsphere. AIP Adv. **4**, 027113 (2014). https://doi.org/10.1063/1.4866446
114. Y. Deng, R.K. Jain, M. Hossein-Zadeh, Demonstration of a cw room temperature mid-IR microlaser. Opt. Lett. **39**, 4458–4461 (2014). https://doi.org/10.1364/OL.39.004458
115. F. Vanier, F. Côté, M.E. Amraoui, Y. Messaddeq, Y.-A. Peter, M. Rochette, Low-threshold lasing at 1975 nm in thulium-doped tellurite glass microspheres. Opt. Lett. **40**, 5227–5230 (2015). https://doi.org/10.1364/OL.40.005227
116. L. Peng, Y. Huang, Y. Duan, S. Zhuang, T. Liao, C. Xu, 2 μm laser oscillation of Ho^{3+}:Tm^{3+}-codoped silica microspheres. Appl. Opt. **56**, 7469–7473 (2017). https://doi.org/10.1364/AO.56.007469
117. Z. Yang, Y. Wu, K. Yang, P. Xu, W. Zhang, S. Dai, T. Xu, Fabrication and characterization of Tm^{3+}–Ho^{3+} co-doped tellurite glass microsphere lasers operating at ∼2.1 μm. Opt. Mater. **72**, 524–528 (2017). https://doi.org/10.1016/j.optmat.2017.06.057
118. Z. Fang, S.N. Chormaic, S. Wang, X. Wang, J. Yu, Y. Jiang, J. Qiu, P. Wang, Bismuth-doped glass microsphere lasers. Photonics Res. **5**, 740–744 (2017). https://doi.org/10.1364/PRJ.5.000740
119. A. Li, J. Yu, M. Zhang, X. Lu, J. Zhang, E. Lewis, G. Farrell, P. Wang, An Yb^{3+}–Ho^{3+} codoped glass microsphere laser in the 2.0 μm wavelength regions. IEEE Photonics Technol. Lett. **30**, 1543–1546 (2018). https://doi.org/10.1109/LPT.2018.2859053
120. X. Wang, Y. Yu, S. Wang, J.M. Ward, S.N. Chormaic, P. Wang, Single mode green lasing and multicolor luminescent emission from an Er^{3+}–Yb^{3+} co-doped compound fluorosilicate glass microsphere resonator. OSA Contin. **1**, 261–273 (2018). https://doi.org/10.1364/OSAC.1.000261

121. A. Li, J. Zhang, M. Zhang, W. Li, S. Wang, E. Lewis, G. Brambilla, P. Wang, Effect of Tm^{3+} concentration on the emission wavelength shift in Tm^{3+}-doped silica microsphere lasers. Opt. Lett. **43**, 4325–4328 (2018). https://doi.org/10.1364/OL.43.004325
122. D. Ristić, A. Chiappini, M. Mazzola, P. Féron, H. Gebavi, M. Ivanda, M. Ferrari, Lasing and mode selection in erbium doped $70SiO_2$–$30HfO_2$ coated microspheres. Opt. Mater. **87**, 98–101 (2019). https://doi.org/10.1016/j.optmat.2018.05.018
123. A. Li, W. Li, M. Zhang, Y. Zhang, S. Wang, A. Yang, Z. Yang, E. Lewis, G. Brambilla, P. Wang, Tm^{3+}–Ho^{3+} codoped tellurite glass microsphere laser in the 1.47 μm wavelength region. Opt. Lett. **44**, 511–513 (2019). https://doi.org/10.1364/OL.44.000511
124. J. Qin, Y. Huang, T. Liao, C. Xu, C. Ke, Y. Duan, 1.9 μm laser and visible light emissions in Er^{3+}/Tm^{3+} co-doped tellurite glass microspheres pumped by a broadband amplified spontaneous emission source. J. Opt. **21**, 035401 (2019). https://doi.org/10.1088/2040-8986/ab0264
125. A. Li, M. Zhang, X. Wang, S. Wang, B. Guo, E. Lewis, P. Wang, Directly pumped Ho^{3+}-doped microspheres lasing at 2.0 μm. IEEE Photonics Technol. Lett. **31**, 1366–1368 (2019). https://doi.org/10.1109/LPT.2019.2927085
126. H.Y. Zhao, A.Z. Li, Y.T. Yi, M. Tokurakawa, G. Brambilla, S.J. Jia, S.B. Wang, P.F. Wang, A Tm^{3+}-doped ZrF_4-BaF_2-YF_3-AlF_3 glass microsphere laser in the 2.0 μm wavelength region. J. Lumin. **212**, 207–211 (2019). https://doi.org/10.1016/j.jlumin.2019.04.046
127. X. Wang, J. Yu, H. Zhao, X. Lu, W. Li, K. Tian, G. Brambilla, P. Wang, 1.88 μm laser emission from Tm^{3+} doped fluorosilicate glass microspheres with excellent stability and high damage threshold. J. Lumin. **220**, 117028 (2020). https://doi.org/10.1016/j.jlumin.2020.117028
128. A. Li, Y. Dong, S. Wang, S. Jia, G. Brambilla, P. Wang, Infrared-laser and upconversion luminescence in Ho^{3+}–Yb^{3+} codoped tellurite glass microsphere. J. Lumin. **218**, 116826 (2020). https://doi.org/10.1016/j.jlumin.2019.116826
129. J. Yu, X. Wang, W. Li, M. Zhang, J. Zhang, K. Tian, Y. Du, S. Nic Chormaic, P. Wang, An experimental and theoretical investigation of a 2 μm wavelength low-threshold microsphere laser. J. Lightwave Technol. **38**, 1880–1886 (2020). https://doi.org/10.1109/JLT.2019.2958349
130. P. Wang, Y. Yi, X. Wang, A. Li, S. Jia, Y. Fan, G. Brambilla, S. Wang, H. Zhao, Tm3+-doped fluorotellurite glass microsphere resonator laser at 23 μm. Opt. Lett. **45**, 3553–3556 (2020). https://doi.org/10.1364/OL.396843
131. Q. Xu, S. Peng, T. Liao, Y. Huang, A stable 1550nm WGM laser generated by Yb^{3+}/Er^{3+} co-doped silica microspheres under μm ASE source pumping. J. Phys. Conf. Ser. **2112**, 012013 (2021). https://doi.org/10.1088/1742-6596/2112/1/012013
132. T. Van Nguyen, T.B. Pham, H. Bui, T. Chi Do, V.H. Pham, Coherent up-conversion in Erbium-doped silica microspheres enhanced by thin-film metal deposition. Photonics Nanostruct. Fundam. Appl. **47**, 100971 (2021). https://doi.org/10.1016/j.photonics.2021.100971
133. M.R. Foreman, J.D. Swaim, F. Vollmer, Whispering gallery mode sensors. Adv. Opt. Photonics **7**, 168–240 (2015). https://doi.org/10.1364/AOP.7.000168
134. J. Yang, L.J. Guo, Optical sensors based on active microcavities. IEEE J. Sel. Top. Quantum Electron. **12**, 143–147 (2006). https://doi.org/10.1109/JSTQE.2005.862953
135. F. Paz-Buclatin, Y. Perera-Suárez, I.R. Martín, S. Ríos, O. de Varona, A. Ródenas, L.L. Martin, Experimental and numerical validation of whispering gallery resonators as optical temperature sensors. Sensors **22**, 7831 (2022). https://doi.org/10.3390/s22207831
136. D.S. Weiss, V. Sandoghdar, J. Hare, V. Lefèvre-Seguin, J.-M. Raimond, S. Haroche, Splitting of high-Q Mie modes induced by light backscattering in silica microspheres. Opt. Lett. **20**, 1835–1837 (1995). https://doi.org/10.1364/OL.20.001835
137. L. He, ŞK. Özdemir, J. Zhu, W. Kim, L. Yang, Detecting single viruses and nanoparticles using whispering gallery microlasers. Nat. Nanotechnol. **6**, 428–432 (2011). https://doi.org/10.1038/nnano.2011.99
138. J.-B. Ceppe, P. Féron, M. Mortier, Y. Dumeige, Dynamical analysis of modal coupling in rare-earth whispering-gallery-mode microlasers. Phys. Rev. Appl. **11**, 064028 (2019). https://doi.org/10.1103/PhysRevApplied.11.064028
139. Y. Kim, H. Lee, H. Lee, On-chip label-free biosensing based on active whispering gallery mode resonators pumped by a light-emitting diode. Opt. Express **27**, 34405–34415 (2019). https://doi.org/10.1364/OE.27.034405